

THE CLUSTERING OF LUMINOUS RED GALAXIES AT $z \sim 0.7$ FROM EBOSS DATA

ZHONGXU ZHAI¹, JEREMY L. TINKER¹, CHANGHOON HAHN¹, HEE-JONG SEO², MICHAEL R. BLANTON¹, RITA TOJEIRO³,
HUGO O. CAMACHO^{4,5}, MARCOS LIMA^{4,5}, AURELIO CARNERO ROSELL^{6,5}, FLAVIA SOBREIRA^{7,5,8}, LUIZ N. DA COSTA^{5,6},
JULIAN E. BAUTISTA⁹, JOEL R. BROWNSTEIN⁹, JOHAN COMPARAT^{10,11}, KYLE DAWSON⁹, JEFFREY A. NEWMAN¹²,
ALEXANDRE ROMAN-LOPES¹³, DONALD P. SCHNEIDER^{14, 15}

Draft version April 30, 2022

ABSTRACT

We present the first scientific results from the luminous red galaxy sample (LRG) of the extended Baryon Oscillation Spectroscopic Survey (eBOSS). We measure the small and intermediate scale clustering from a sample of more than 61,000 galaxies in the redshift range $0.6 < z < 0.9$. We interpret these measurements in the framework of the Halo Occupation Distribution. The bias of eBOSS LRGs is 2.30 ± 0.03 , with a satellite fraction of $13 \pm 3\%$ and a mean halo mass of $2.5 \times 10^{13} h^{-1} M_{\odot}$. These results are consistent with expectations, demonstrating that eBOSS galaxies will be reliable tracers of large scale structure at $z \sim 0.7$. The eBOSS galaxy bias implies a scatter of luminosity at fixed halo mass, $\sigma_{\log L}$, of 0.19 dex. Using the clustering of massive galaxies from BOSS-CMASS, BOSS-LOWZ, and SDSS, we find that $\sigma_{\log L} = 0.19$ is consistent with observations over the full redshift range that these samples cover. The addition of eBOSS to previous surveys allows investigation of the evolution of massive galaxies over the past ~ 7 Gyr.

Subject headings: large scale structure of universe

1. INTRODUCTION

Galaxy redshift surveys have been fundamental in advancing our understanding of the universe. The successes of the past decade, varying from 2dFGRS (Cole et al. 2005), SDSS (Eisenstein et al. 2005; Zehavi et al. 2011), and BOSS (Anderson et al. 2012), have spawned even larger investments in mapping the universe through the three-dimensional distributions of galaxies. In this paper, we present the first measurements of the clustering of luminous red galaxies (LRGs) from the extended

Baryon Oscillation Spectroscopic Survey (eBOSS; Dawson et al. 2016), the successor program to BOSS (Dawson et al. 2013). The eBOSS LRG program has the power to provide reliable measurements of galaxy clustering.

We focus on LRG clustering at small scales ($r \lesssim 20 h^{-1}$ Mpc), scales which provide information on the bias of the galaxy sample and how these galaxies are distributed in dark matter halos. The framework in which we interpret the eBOSS data is the Halo Occupation Distribution (HOD). This approach describes the bias relation between the galaxies and matter at the level of “virialized” dark matter halos which are expected to be in approximate dynamical equilibrium (Berlind & Weinberg 2002; Peacock & Smith 2000; Seljak 2000; Benson et al. 2000; White et al. 2001; Cooray & Sheth 2002). In the HOD framework, the key quantity is the probability distribution $P(N|M)$ that a halo of virial mass M contains N galaxies of a given type, along with the relations between the galaxy and dark matter spatial and velocity distributions within halos. Given an HOD and a particular cosmological model, the statistics of galaxy clustering can be predicted in the sense that the cosmological model determines the properties of the halo distribution, while the HOD specifies how those halos are populated with galaxies. HOD modeling has been used to interpret clustering in nearly all large-scale galaxy redshift surveys (e.g. Zheng et al. 2007; Zheng et al. 2009; Zehavi et al. 2011; White et al. 2011; Parejko et al. 2013; Guo et al. 2014). The HOD results provide physically informative and important information to test theories of galaxy formation and evolution.

One of the key quantities in galaxy formation is the scatter in galaxy luminosity (or stellar mass) at fixed halo mass. Clustering is one of the few methods that is sensitive to the scatter. We will use the HOD to estimate this scatter and compare it to other galaxy samples spanning a redshift range of $z = 0.7$ to $z = 0.1$. We will show that this scatter is both small (0.19 dex in $\log L$)

¹ Center for Cosmology and Particle Physics, Department of Physics, New York University, 4 Washington Place, New York, NY 10003, USA.

² Department of Physics and Astronomy, Ohio University, 251B Clippinger Labs, Athens, OH 45701.

³ Institute of Cosmology & Gravitation, Dennis Sciama Building, University of Portsmouth, Portsmouth, PO1 3FX, UK.

⁴ Departamento de Física Matemática, Instituto de Física, Universidade de São Paulo, CP 66318, CEP 05314-970, São Paulo, SP, Brazil

⁵ Laboratório Interinstitucional de e-Astronomia, 77 Rua Gal. José Cristino, Rio de Janeiro, RJ - 20921-400, Brazil.

⁶ Observatório Nacional, 77 Rua Gal. José Cristino, Rio de Janeiro, RJ - 20921-400, Brazil.

⁷ Universidade Federal do ABC, Centro de Ciências Naturais e Humanas, Av. dos Estados, 5001, Santo André, SP, Brazil, 09210-580

⁸ Instituto de Física Teórica, Universidade Estadual Paulista, Rua Dr. Bento T. Ferraz, 271, São Paulo, SP, 01140-070, Brazil

⁹ Department of Physics and Astronomy, University of Utah, Salt Lake City, UT 84112, USA.

¹⁰ Instituto de Física Teórica UAM/CSIC, 28049 Madrid, Spain.

¹¹ Departamento de Física Teórica, Universidad Autónoma de Madrid, 28049 Madrid, Spain.

¹² Department of Physics and Astronomy and PITT PACC, University of Pittsburgh, Pittsburgh, PA 15260, USA.

¹³ Departamento de Física, Facultad de Ciencias, Universidad de La Serena, Cisternas 1200, La Serena, Chile.

¹⁴ Department of Astronomy and Astrophysics, The Pennsylvania State University, University Park, PA 16802.

¹⁵ Institute for Gravitation and the Cosmos, The Pennsylvania State University, University Park, PA 16802.

and constant over this redshift range.

Our paper is organized as follows. Section 2 briefly describes the eBOSS observations and the definition of our LRG sample. The measurement of clustering is presented in Section 3, along with the comparison with the BOSS result. In Section 4, we interpret our result in the framework of HOD. Finally, the conclusion and discussion of our measurements as well as its implication are given in Section 5. Throughout this paper, the distances are measured in units of h^{-1} Mpc with the Hubble constant $H_0 = 100 h \text{ km s}^{-1} \text{ Mpc}^{-1}$. The redshifts are converted to distances by assuming a spatially flat Λ CDM model with $(\Omega_m, h) = (0.29, 0.7)$. The same cosmology is also used for the N -body simulations to make mock catalogs. The halos are defined as the spherical overdensity masses which are 200 times the background density.

2. OBSERVATIONS AND DATA

Motivated by the success of BOSS (Bolton et al. 2012; Dawson et al. 2013; Eisenstein et al. 2011; Gunn et al. 2006; Smee et al. 2013), eBOSS will explore a larger volume and higher redshift of the universe (Dawson et al. 2016). As a six-year program, the primary scientific goals of eBOSS are to provide the first high precision measurements of baryon acoustic oscillations (BAO) and redshift space distortions (RSD) in the redshift range $0.6 < z < 2.0$ (Zhao et al. 2016). Measurements of the expansion history in this redshift range contain important information about the transition from cosmic deceleration to acceleration. Here, we focus on the eBOSS LRG sample, which extends the BOSS galaxy sample to higher redshift, probing the range $0.6 < z < 1.0$ with a target density of 60 deg^{-2} . The LRG target selection is based on *ugriz* (Fukugita et al. 1996) SDSS imaging data combined with infrared photometry from Wide-Field Infrared Survey Explorer (WISE; Wright et al. 2010). The use of infrared data allows selections of fainter optical targets at higher redshift while minimizing stellar contamination of the sample. A full description of the target selection algorithm, including tests for systematics, is presented in Prakash et al. (2016).

The eBOSS LRG target selection imposes a bright limit of $i = 19.9$, making the eBOSS sample nearly complementary to the BOSS CMASS sample, which used SDSS imaging only to probe the redshift range $0.4 < z < 0.7$. For the clustering analysis in this paper, we combine the eBOSS LRGs with the high-redshift tail of the CMASS sample. The motivation for this combination is two fold: (1) HOD analysis typically assumes that a sample of galaxies is complete, in the sense that it includes all galaxies above some mass or luminosity threshold. (2) The cosmology analysis with eBOSS is likely to merge the two catalogs; this increases the density of the sample without decreasing the median redshift.

Figure 1 shows the distribution of i -band magnitude as a function of redshift for both BOSS-CMASS and eBOSS LRGs. At $z < 0.75$, the complementarity of the eBOSS and BOSS samples is clear, with BOSS populating the bright end of the distribution. The slight overlap between BOSS and eBOSS galaxies is due to the bright limit in eBOSS using “model” magnitudes, while the faint limit in CMASS was enforced with “cmodel” magnitudes (see Stoughton et al. 2002; Abazajian et al. 2004, for details of the magnitudes and further discussion). The smaller

scatter between these two quantities causes some overlap in the i -band distribution. At $z > 0.75$, the combined sample is dominated by eBOSS galaxies due to the flux limit of BOSS.

The space density of the eBOSS, BOSS, and the combined sample is shown in Figure 2. Dotted lines indicate our fiducial redshift range. Within this range, the fraction of all galaxies that are eBOSS LRGs is about 60%. The combination of the eBOSS sample with the flux-limited tail of the CMASS distribution makes for a highly asymmetric $n(z)$, but we will demonstrate in Section 4.1 that our halo occupation results are insensitive to the exact details of the galaxy number density.

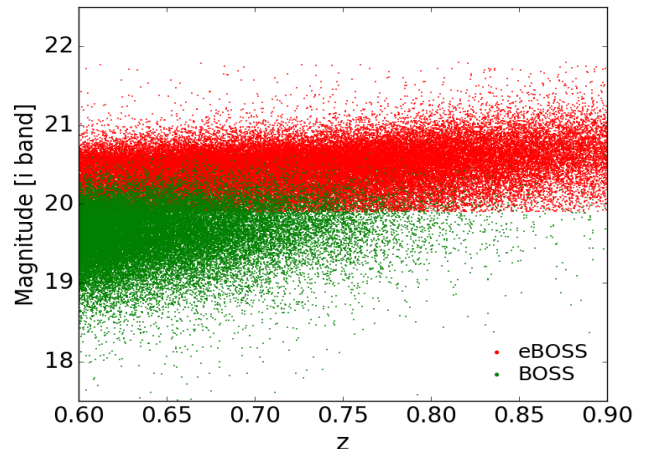


FIG. 1.— The distribution of the i -band model magnitude after the correction of galactic extinction *versus* redshift for the eBOSS (red) and BOSS (green) samples.

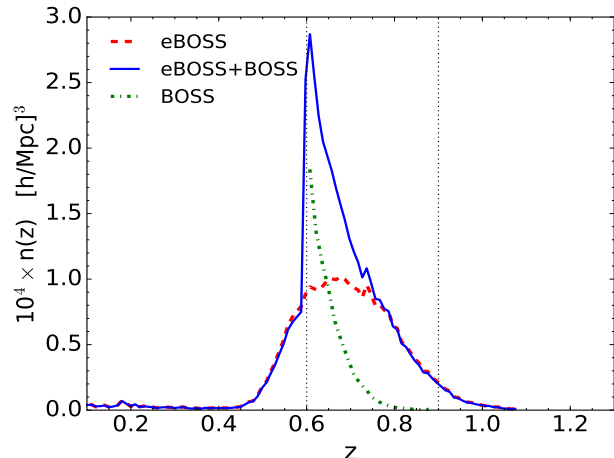


FIG. 2.— The number density of the galaxies for the sample described in the text. The data used for the clustering measurement are restricted between the vertical dashed lines at $z = 0.6$ and $z = 0.9$.

The clustering measurements in this paper are based on the eBOSS DR14 LRG data taken prior to May 2016. This sample yields a total number of spectra of 110,000

and an areal coverage of 1591 deg^{-2} . We restrict the data to the sectors with a completeness greater than 0.5 and then select the galaxies in our redshift range. The overall completeness in each sector is defined as

$$C = \frac{N_{\text{spec}} + N_{\text{cp}} + N_{\text{BOSS}} + N_{\text{BOSS}_{\text{cp}}}}{N_{\text{targ}} - N_{\text{star}} - N_{\text{knocks}} + N_{\text{BOSS}} + N_{\text{BOSS}_{\text{cp}}}}, \quad (1)$$

where N is the number of objects in the sector, **spec** denotes galaxies with good eBOSS spectra, **cp** denotes objects with no spectra, because they were too close to another LRG target to assign a fiber—the well-known “fiber collision” effect, **BOSS** denotes BOSS galaxies with spectra, **BOSS_{cp}** has the same meaning as **cp** but in the BOSS-CMASS sample, **targ** denotes targets, **star** denotes spectroscopically confirmed stars, and **knocks** denotes knockouts from higher priority targets which we will discuss in more detail presently. In the analysis, we define “good” eBOSS spectra as follows,

$$\begin{aligned} & (1) \text{SPECPRIMARY} == 1, \quad \text{AND} \\ & \left((2a) \text{ZWARNING_NOQSO} == 0, \quad \text{OR} \right. \quad (2) \\ & \quad \left. (2b) \text{ZWARNING_NOQSO} == 2^2 \text{ AND} \right. \\ & \quad \left. 0.005 < \text{RCHI2DIFF_NOQSO} < 0.01 \right) \end{aligned}$$

These parameters are the flags in the eBOSS catalogue: **SPECPRIMARY** identifies the best spectrum among multiple observations, **ZWARNING_NOQSO** lists potential problems with the redshift fit and a value of 0 denotes no obvious problems, **RCHI2DIFF_NOQSO** is the difference of reduced χ^2 between the best-fit and second best-fit templates. The third condition is used to relax the threshold of **ZWARNING_NOQSO** = 2^2 , since in Dawson et al. (2016) it was shown that the catastrophic failure rate is still below 1% for **RCHI2DIFF_NOQSO** > 0.005. Future analysis of clustering with the eBOSS LRG sample will likely use the redshift estimates derived from a new spectroscopic classification algorithm (Hutchinson et al. 2016). The new routine is based on a least squares fit against discrete, physically-motivated spectral templates rather than against a linear combination of templates derived from principal component analysis as was done in BOSS redshift classification (Bolton et al. 2012). The new redshift classification algorithm has been shown to produce a higher fraction of reliable redshift estimates, particularly in the presence of stellar contamination and low signal-to-noise spectra. The above approach increases the redshift success rate by about 15%. These criteria yield an eBOSS LRG sample of 61,000 galaxies, and the redshift success rate is 84%. The stellar fraction in the spectroscopic sample is found to be about 11%. We restrict the CMASS galaxies to the same footprint as the eBOSS sample resulting in an eBOSS+BOSS sample of 97,000 galaxies. Figure 3 displays the sky coverage of the eBOSS LRG sample color-coded by completeness. The North Galactic Cap (NGC) and South Galactic South (SGC) are analyzed jointly for simplicity. The area covered by the survey and the angular completeness of each sector is tracked by the **MANGLE** software (Swanson et al. 2008).

We apply additional masks to the data to account for various systematics. During fiber assignment, LRGs are

only given access to fibers after all other targets have been through fiber allocation. Thus, there is a significant amount of area that is “not viewable” from the point of view of the LRGs due to fiber collisions — the limit that two fibers cannot be closer than $62''$ on a given plate; see Dawson et al. (2016) for full details. LRG targets that are within the collision radius of a high priority target are designated knockouts (the collision of a LRG with another LRG will be discussed later). Some knockouts are recovered in plate overlaps, but in total roughly 10% of the LRG footprint is eliminated due to this effect. We create a collision priority mask to remove both targets and randoms from this area. Bright stars in WISE can also impact target selection. In our fiducial results, we do not use the bright star mask, but we demonstrate that it has negligible effect on our clustering measurement in Appendix A.

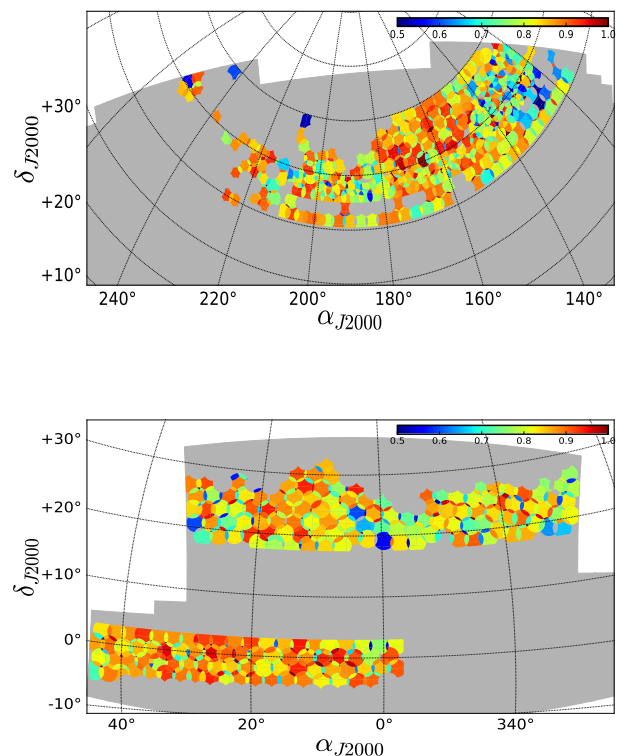


FIG. 3.— The sky coverage of the galaxy sample used in this analysis, in the Lambert azimuthal equal-area projection. The light grey region shows the expected total footprint of the survey, while the colors indicate the completeness in each sector. The mean completeness in each sector is 0.8, the weighted area of the current footprint is 827 deg^2 for NGC (top) and 763 deg^2 for SGC (bottom) respectively.

3. CLUSTERING MEASUREMENTS

The primary tool to study the statistics of the galaxy distribution is the two-point correlation function $\xi(r)$, which measures the excess probability of finding galaxy pairs over a random sample of points as a function of separation r (Peebles 1980). In order to account for the redshift space distortions caused by the galaxy peculiar

velocities, it is convenient to calculate the correlation function on a two-dimensional grid of pair separations perpendicular (r_p) and parallel (π) to the line of sight. For a pair of galaxies with redshift space positions \mathbf{s}_1 and \mathbf{s}_2 , the dependence of the correlation function is only through $\mathbf{s} = \mathbf{s}_1 - \mathbf{s}_2$ and the orientation of \mathbf{s} relative to the line-of-sight. In this case, we may write the $\xi(r)$ as $\xi(\pi, r_p)$ through the relation

$$\pi = \frac{\mathbf{s} \cdot \mathbf{l}}{|\mathbf{l}|}, \quad r_p^2 = \mathbf{s} \cdot \mathbf{s} - \pi^2, \quad r^2 = \mathbf{s} \cdot \mathbf{s}, \quad (3)$$

with $\mathbf{l} = (\mathbf{s}_1 + \mathbf{s}_2)/2$ (e.g. Davis & Peebles 1983; Fisher et al. 1994).

The calculation of the correlation function from the galaxy sample is through the estimator (Landy & Szalay 1993)

$$\xi(r_p, \pi) = \frac{DD - 2DR + RR}{RR}, \quad (4)$$

where DD , DR , and RR are suitably normalized numbers of (weighted) data-data, data-random, and random-random pairs in each separation bin.

In order to mitigate the effect of redshift space distortion and examine the real space correlation function, we compute the projected correlation function from $\xi(r_p, \pi)$ (Davis & Peebles 1983)

$$w_p(r_p) = 2 \int_0^\infty d\pi \xi(r_p, \pi). \quad (5)$$

In practice, the integral of π can be up to $80 h^{-1}\text{Mpc}$, which is large enough to include most of the correlated pairs and produce a stable result. The measurement of $w_p(r_p)$ is achieved with 10 equally spaced bins in $\log r_p$ from $0.2 h^{-1}\text{Mpc}$ to $60 h^{-1}\text{Mpc}$.

Fiber collisions between LRG-LRG pairs reduce the spectroscopic completeness by $\sim 5\%$ ¹⁶, and these collisions have an impact on both the measured large-scale bias and the small scale clustering. We correct this effect by combining two different weights: (1) upweighting galaxies which have a fiber assigned in the collided-pairs and (2) reconstructing the correct galaxy pair counts in scales smaller than $62''$. The first weighting scheme is similar to the “nearest-neighbor method” and corrects for the impact of collisions on the bias (Zehavi et al. 2002, 2005). The second scheme corrects the clustering amplitude at small scales by using the ratio of angular correlation functions (Hawkins et al. 2003)

$$F(\theta) = \frac{1 + w_z(\theta)}{1 + w_t(\theta)}, \quad (6)$$

where $w_z(\theta)$ is the angular correlation function of galaxies drawn from the “spectroscopic” sample which has fibers assigned, and $w_t(\theta)$ is the angular correlation function for the entire photometric sample.

The quantity $1 + w(\theta)$ is proportional to the number of pairs at angle θ , thus we weight each DD pair in Eq. (4) by $1/F(\theta)$ to account for the loss of pairs due to collisions. Figure 4 presents this angular correction for

both eBOSS and BOSS galaxy samples used in our analysis. The ratio is close to unity above the fiber collision scale but depressed significantly at separations below this scale. To interpret these data we start with results from BOSS. For fiber allocation in BOSS, the mandate was to place a fiber on every galaxy possible—i.e., to achieve 100% completeness in the ‘decollided’ set¹⁷. Thus, in areas of the survey covered by more than one tile, all collisions were resolved by observing one galaxy on each plate. Because 40% of BOSS was covered by more than one tile, the value of F at $\theta < 62''$ is 0.4. The value of F for eBOSS galaxies is substantially smaller below the collision scale, in spite of the fact that the multi-tile coverage is nearly the same. Indeed, when measuring $F(\theta)$ in regions of eBOSS covered by more than one tile, $F(\theta)$ is still substantially below unity.

The reason for the different results between BOSS and eBOSS lies in the fiber allocation priorities. In BOSS, the goal of 100% completeness in the decollided set was met at the expense of some unused fibers, which totalled 7%. To maximize fiber usage in eBOSS, the goal of 100% decollided completeness was relaxed for the LRGs (but only for the LRGs). Due to fluctuations in the density of higher priority targets, the number of LRG fibers varied from plate to plate. Thus, in some plates, there exist more LRG targets than available fibers. This effects a small fraction of area; 90% of the eBOSS footprint placed fibers on $\geq 90\%$ of available LRG targets (cf. Figure 4 in Dawson et al. 2016). However, the fiber allocation algorithm prioritizes galaxies in the decollided set. Thus, if a plate runs out of fibers before all available LRGs could be assigned, the set of LRGs left unassigned are preferentially in pairs. Correcting for this effect, fortunately, is identical to our standard method of correcting for fiber collisions; this result is shown explicitly on mock data in Appendix B.

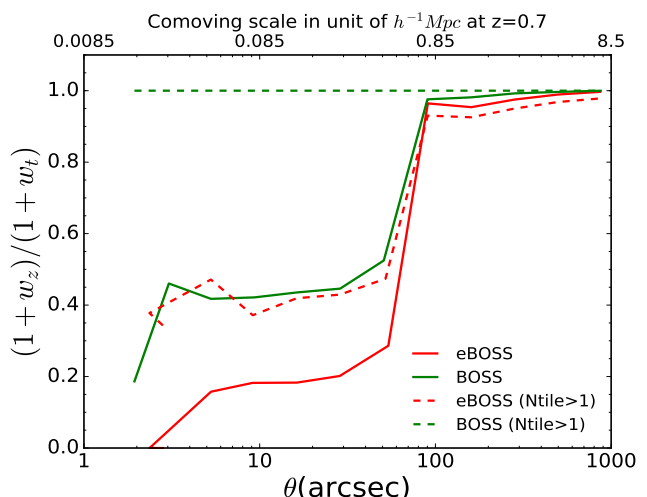


FIG. 4.— The angular correction (Eq.6) for eBOSS (red) and BOSS (green) samples in the pair counts to calculate the correlation function. $N_{\text{tile}} > 1$ refers to sectors that are observed more than once. This quantity is used to weight the galaxy pairs to account for the loss of pairs due to collisions.

¹⁶ This is a distinct effect from knockouts, where LRGs cannot be assigned fibers due to collisions with other—uncorrelated—samples of targets. This effect is specifically caused by the collision between two LRGs.

¹⁷ The decollided set contains all targets that are not within collision groups (groups of targets that lie within $62''$ of one another), combined with the subset of collided targets that can be assigned fibers on a single plate (Dawson et al. 2016).

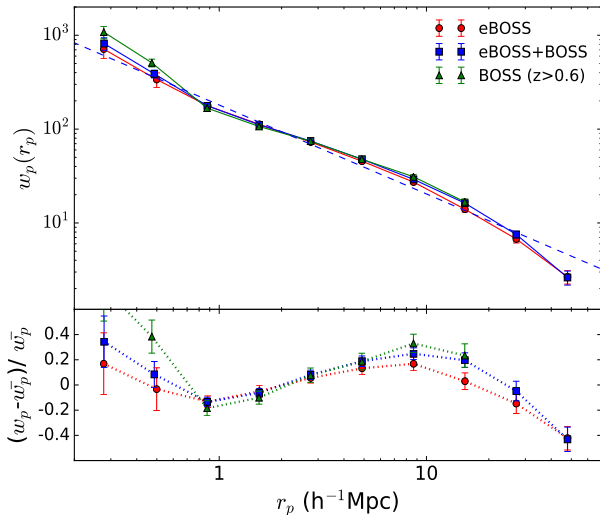


FIG. 5.— *Top panel:* Projected correlation function for the eBOSS, BOSS and eBOSS+BOSS LRG samples. The dashed line corresponds to the best-fit power law for eBOSS LRGs $w_p(r_p) \propto r_p^{1-\gamma}$ with $\gamma \sim 1.95$. *Bottom panel:* The fractional difference for the two samples with respect to the best-fit power law function. Note that the two data points at the largest scale for BOSS w_p are not shown, because they are negative due to the sample variance which is mainly introduced by restricting the BOSS CMASS galaxies within the eBOSS footprint.

Our measurement of $w_p(r_p)$ is shown in Figure 5 for CMASS, eBOSS LRGs, and the combined sample. Note again that we restrict the CMASS sample to be within the same eBOSS survey area and redshift range. The angular completeness and the radial selection function are calculated for eBOSS and eBOSS+BOSS independently, and the angular upweighting correction is also applied to eBOSS and BOSS LRGs separately. Specifically, in the combined sample, a BOSS-BOSS pair at $\theta < 62''$ is upweighted by 2.64, while an eBOSS-eBOSS pair is upweighted by 5.1, and all eBOSS-BOSS cross pairs are not upweighted because there are no collisions between surveys. The clustering measurements from eBOSS are in agreement with earlier measurements of massive galaxies at lower redshift (White et al. 2011; Parejko et al. 2013).

The errors in the clustering measurements can be estimated in multiple ways (Norberg et al. 2009). The eBOSS survey is far from complete, therefore the relatively small sky coverage and the irregular geometry (Figure 3) may introduce some difficulties in calculating the covariance matrix from the resampling methods, such as jackknife and bootstrap (White et al. 2011). We compute the covariance from 100 independent mock catalogs created from the quick particle mesh method (QPM; White et al. 2014). These mock catalogs have the same angular selection function and $n(z)$ as the data. They do not include fiber collisions or fiber allocation effects, so we increase the variance from the mocks by $1/F(\theta)$ at $\theta < 62''$ to account for the larger shot noise in the data at small scales. In practice, we require an HOD model to make mock catalogs: we perform a ‘first-pass’ HOD analysis on the data (see §2) assuming constant fractional errors in $w_p(r_p)$. The resulting HOD is used

to populate the mock catalogs, which are then used to perform our final HOD analysis on the data. The resulting correlation matrix for eBOSS+BOSS sample is presented in Figure 6. The error bars of $w_p(r_p)$ measurements in Figure 5 are related to the diagonal elements of the covariance matrix. As expected, the $w_p(r_p)$ data are highly correlated at $r_p \gtrsim 2 h^{-1}\text{Mpc}$, where pairs of galaxies come from two distinct halos, while at smaller scales galaxy pairs reside in a single halo which is dominated by uncorrelated shot noise.

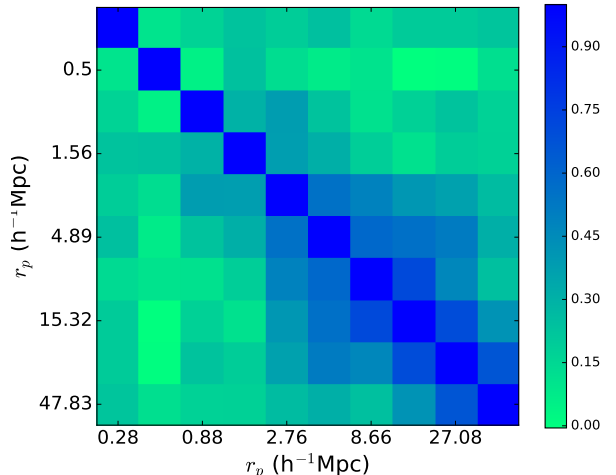


FIG. 6.— The correlation matrix for the clustering measurements from the eBOSS+BOSS LRG sample. It is calculated from 100 independent mock catalogs by the use of the particle mesh method. This matrix is used to perform the HOD analysis in Section 4.1

4. ANALYSIS

4.1. HOD modeling

We interpret the observed clustering of galaxies in the framework of the HOD which approaches the problem of galaxy bias statistically. In its most basic form, the HOD constructs a probability distribution $P(N|M)$: the probability that a halo of mass M contains N galaxies of a given class. Here, the class of galaxies is the combined eBOSS+BOSS sample. Because the clustering, abundance, and interior structure of dark matter halos is well known from simulations, specifying $P(N|M)$ essentially provides a complete description of the spatial distribution of galaxies. For HOD parameterization, it is customary to separate the contribution of the central galaxies from that of the satellite galaxies with the mean occupancy of halos:

$$N(M) = \langle N_{\text{gal}}(M) \rangle = N_{\text{cen}}(M) + N_{\text{sat}}(M). \quad (7)$$

The mean number of the central galaxies in each halo is modeled with a smooth transition between 0 and 1 galaxy:

$$N_{\text{cen}}(M) = \frac{1}{2} \left[1 + \text{erf} \left(\frac{\log M - \log M_{\text{min}}}{\sigma_{\log M}} \right) \right], \quad (8)$$

TABLE 1
THE MEAN AND STANDARD DEVIATION OF THE HOD PARAMETERS
FROM THE MARKOV CHAIN ANALYSIS.

	eBOSS+BOSS	best-fit
$\log M_{\min}$	$13.68^{+0.06}_{-0.05}$	13.67
$\log M_{\text{sat}}$	$14.87^{+0.60}_{-0.32}$	14.93
α	$0.41^{+0.20}_{-0.16}$	0.43
$\log M_{\text{cut}}$	$12.32^{+0.76}_{-0.88}$	11.62
$\sigma_{\log M}$	0.82 ± 0.05	0.81
b	2.30 ± 0.03	2.31
f_{sat}	$13.0 \pm 3.0\%$	15.2%
χ^2	—	14.71

and the mean number of satellite galaxies is parameterized as

$$N_{\text{sat}}(M) = \left(\frac{M}{M_{\text{sat}}} \right)^{\alpha} \exp \left(-\frac{M_{\text{cut}}}{M} \right) N_{\text{cen}}(M). \quad (9)$$

Multiplying the central galaxy occupation function in this form guarantees that the satellite occupation terminates at a mass higher than the central occupation cutoff. In this HOD model, M_{\min} , $\sigma_{\log M}$, α , M_{sat} and M_{cut} are the free parameters to be fit by observations which include both $w_p(r_p)$ and the observed number density of galaxies. Briefly, M_{\min} is the mass at which half the halos have a central galaxy, $\sigma_{\log M}$ physically relates to the scatter of halo mass at fixed galaxy luminosity, α is the power-law index for the mass dependence of the number of satellites, M_{sat} is a typical mass for halos to host one satellite, and M_{cut} allows for the cutoff in the satellite occupation function to vary with halo mass. Different functional forms of the HOD parameterization have been applied in the literature, but the model in Eqs. 7 to 9 is flexible enough to satisfy our requirement. The exploration of the parameter space for the HOD model is performed using the Markov Chain Monte Carlo (MCMC) method. We use the analytic model described in Tinker et al. (2005); Tinker et al. (2012) to calculate w_p from a given HOD model. We note that the eBOSS+BOSS galaxy sample is not an ideal sample for HOD analysis. There are gaps in color space between the selection functions for each sample, thus this sample is not ‘complete’ as is usually assumed in the standard HOD formalism. However, adding BOSS galaxies to eBOSS makes the sample significantly more complete than it would otherwise be. The bright limit on eBOSS target selection implies that the most massive halos are not represented in the sample, and the mean number of galaxies per halo cannot be assumed to monotonically increase. Inclusion of the BOSS sample brings these halos back into the fold, and meets the assumptions inherent in Eq. 8.

The constraints on the HOD parameters are presented in Figure 7 based on χ^2 from the Gaussian likelihood function. M_{\min} is not a free parameter once the galaxy number density \bar{n} is known and the other HOD parameters are specified. In particular, M_{\min} is determined by matching the number density \bar{n} to the integral

$$\bar{n} = \int \frac{dn}{dM} N(M), \quad (10)$$

where dn/dM is the halo mass function from Tinker et al. (2008). The dark matter halo is described by the NFW

profile (Navarro et al. 1996), and the concentration mass relation is adopted from Macciò et al. (2008). The values of the HOD parameters and the statistics with their confidence intervals are given in Table 1.

The top panel of Figure 8 shows the mean occupation function of the best fit model and its uncertainties from the MCMC analysis. The mean halo mass for eBOSS+BOSS sample is $2.5 \times 10^{13} h^{-1} M_{\odot}$, which is roughly in agreement with the CMASS result (White et al. 2011). The bottom panel displays the probability that a galaxy in our sample is hosted by a halo of mass M . The galaxies observed in the survey live in a wide halo mass distribution.

The best-fit of the w_p from the HOD modeling is presented in Figure 9, where the one-halo term and two-halo term are also shown for illustration¹⁸. The transition scale from one-halo term to two-halo term is observed at $\sim 1.2 h^{-1}$ Mpc.

The HOD modeling of massive galaxies at different redshifts has been investigated with various samples and HOD models. We compare our measurements of HOD parameters M_{\min} and M_{sat} versus galaxy number density \bar{n} , with other studies which use the similar statistical method, in Figure 10; these include the samples of SDSS (Zehavi et al. 2011), BOSS CMASS (White et al. 2011), and BOSS LOWZ (Parejko et al. 2013). Our HOD fitting results are in reasonable agreement with those of previous studies. The value of M_{sat} from our eBOSS+BOSS measurement appears to be somewhat above the trend. A larger satellite mass scale would normally imply a smaller fraction of satellites, but the f_{sat} value from eBOSS+BOSS is in good agreement with CMASS and LOWZ results, all near 10%. For these BOSS results, as well as the SDSS results, α is near unity, while our best-fit value is 0.45. There is a strong degeneracy between α and M_{sat} (see Figure 7), such that a value of $\alpha \sim 1$ from the eBOSS+BOSS sample would bring M_{sat} into better agreement with the other surveys.

Zehavi et al. (2011) estimate that $M_{\text{sat}} \approx 17 M_{\min}$ in the SDSS galaxy sample. Incorporating the mass estimates presented in Figure 10, we find this relationship depends on number density as $M_{\text{sat}} \approx 17 M_{\min} (\bar{n}/\bar{n}_{\text{SDSS}})^{0.2}$, where \bar{n}_{SDSS} is the number density of SDSS galaxy samples. This result implies that in the low space density environment, the gap between the masses of the halos which host two galaxies and the one hosting only one galaxy is smaller than in the dense environment.

Based on the HOD fitting, we estimate the bias of the galaxy sample with respect to the dark matter distribution through

$$b = \bar{n}^{-1} \int_0^{\infty} b_h(M) N(M) \frac{dn}{dM} dM, \quad (11)$$

where $b_h(M)$ is the halo bias factor from Tinker et al. (2010), and there is no radial range in which to measure the galaxy bias. The large scale bias of eBOSS+BOSS sample is 2.30 ± 0.03 from our clustering measurements. This value varies inversely with the assumed mass perturbation amplitude σ_8 , which is set to be 0.8 in this

¹⁸ The one-halo term means that the two galaxies in the pair come from the same halo, while the two-halo term means they come from two distinct halos.

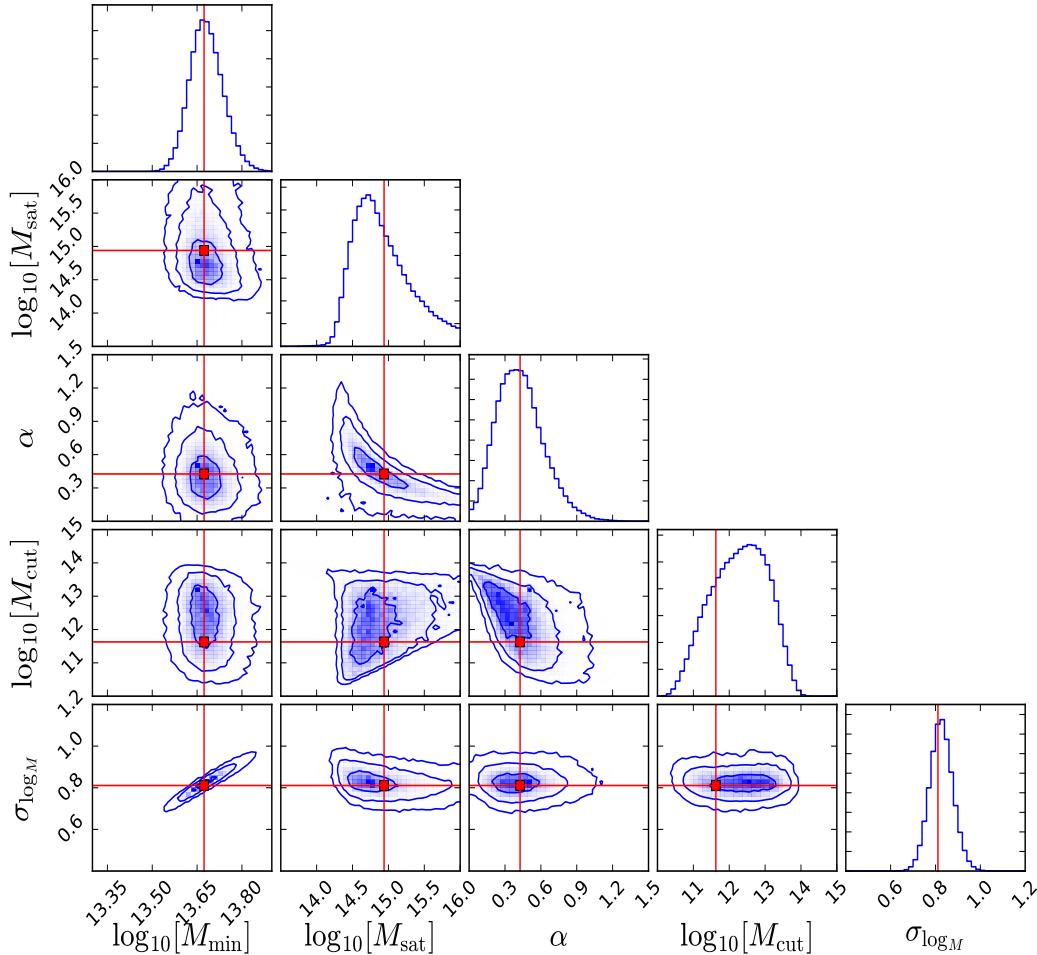


FIG. 7.— The 68%, 95% and 99% confidence intervals of the HOD parameters for the eBOSS+BOSS LRG sample based on the MCMC analysis. The diagonal panels display the one-dimensional probability distribution function. The mass parameters have the unit of $h^{-1}M_{\odot}$, and the red cross stands for the best-fit.

work.

As a consistency check, we have also determined the galaxy bias independently by simply taking the ratio of the measured projected correlation and the theoretical linear dark matter projected correlation. Here we considered only points well within the linear regime ($r_p > 3$ Mpc/h). This method is independent of the HOD modeling and fit details, and yet produces nearly the same best-fit bias, which is reassuring of our methodology.

The above measurements are obtained by the use of the galaxy number density $\bar{n} = 1.4 \times 10^{-4} (h^{-1} \text{Mpc})^{-3}$, which corresponds to the space density at $z = 0.7$ for eBOSS+BOSS sample. We also repeat the analysis for the use of the maximal space density which is about twice the current one. The measurements are not sensitive to the choice of the number density; the satellite fraction increases by 1%, while the bias remains the same. The high χ^2 of the best-fit model, 14.71, is driven by relatively poor agreement with the data at $1 < r_p < 3 h^{-1} \text{Mpc}$. This is likely a failure of the scale-dependent bias model used, which is calibrated on lower-mass halos and lower-redshift samples, and is the chief uncertainty in HOD fitting (see, e.g., Tinker et al. 2012).

4.2. Redshift Evolution

The bias from the eBOSS+BOSS sample is significantly larger than the BOSS results of White et al. (2011) and Parejko et al. (2013). To make a robust comparison between various samples, we compare our eBOSS bias measurement to galaxy samples from BOSS CMASS (White et al. 2011, $z \sim 0.57$), BOSS LOWZ (Parejko et al. 2013, $z \sim 0.3$) and the SDSS Main Galaxy Sample (Zehavi et al. 2011, $z \sim 0.1$) at fixed number density. For each sample, we rank-order the galaxies by i -band absolute magnitude and truncate the sample at the magnitude limit that achieves a space density of $\bar{n}_g = 1.4 \times 10^{-4} (h^{-1} \text{Mpc})^{-3}$. For the CMASS and LOWZ samples, we also restrict the redshift range of the samples to be $\Delta z = \pm 0.13$ and ± 0.1 around the median redshifts respectively. This makes the samples ‘volume-limited’ in an approximate manner. For CMASS and LOWZ, this procedure retains 45% and 50% of the samples. For the SDSS Main Galaxy Sample, we create a volume-limited sample with $M_r < -21.7$ galaxies to obtain the same number density. For each sample, we measure the new bias. Removing the fainter $\sim 50\%$ of each sample has the effect of increasing the measured bias relative to those measured for the full samples. The new bias values are

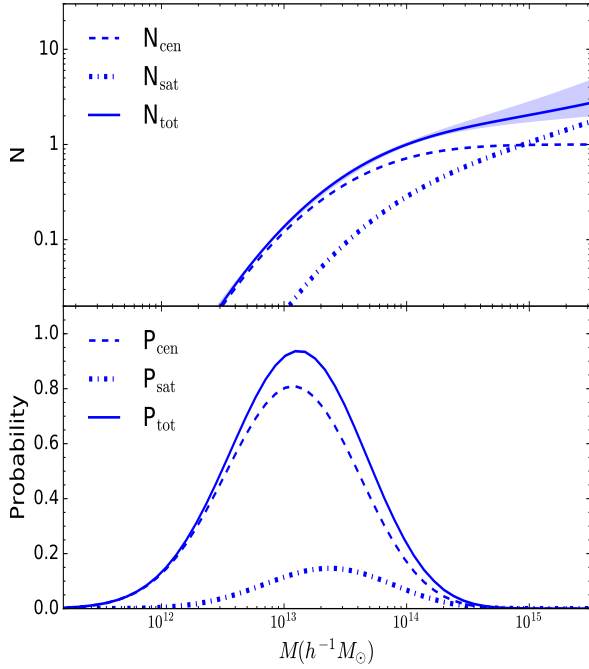


FIG. 8.— *Top panel* : The mean occupancy of halos as a function of halo mass for the eBOSS+BOSS sample used in our calculation. The dashed, dotted and solid lines are N_{cen} , N_{sat} and N respectively. The shaded regions correspond to $\pm 1\sigma$ errors from the MCMC test. *Bottom panel* : Probability per $\log_{10} M$ that a galaxy in our sample is hosted by a halo of mass M . Central and satellite galaxies are shown explicitly.

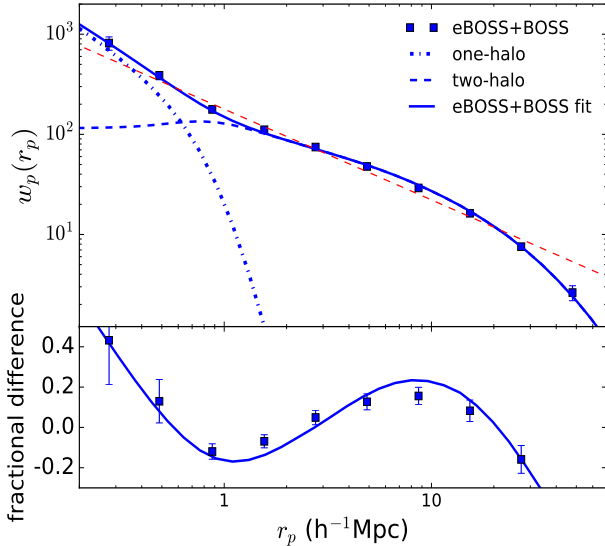


FIG. 9.— *Top panel* : The best-fit of $w_p(r_p)$ from MCMC for eBOSS+BOSS LRG samples, the one-halo term (dash-dotted) and two-halo term (dashed) are shown separately. The red dashed line is the best-fit power-law function. *Bottom panel* : The fractional difference of the clustering data and best-fit with respect to the power-law function. The best-fit χ^2 is 14.71 for $N_d - N_p = 7$ degrees of freedom.

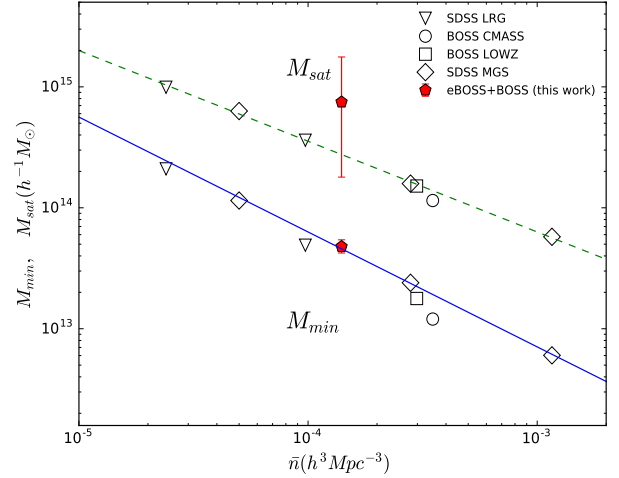


FIG. 10.— The HOD parameters M_{sat} and M_{min} as a function of galaxy number density for different galaxy samples. The error bars are not shown for clarity except for the eBOSS+BOSS results. The labels refer to following studies: SDSS LRG: Zheng et al. (2009), BOSS CMASS: White et al. (2011), BOSS LOWZ: Parejko et al. (2013), SDSS MGS: Zehavi et al. (2011), eBOSS and eBOSS+BOSS: this work. The solid and dashed lines roughly show the linear tendency of M_{min} and M_{sat} with respect to the number density.

shown as a function of redshift in Figure 11. When fixing \bar{n}_g , the $b(z)$ results show a fairly linear trend with redshift, opposed to the full-sample BOSS analysis that found $b \sim 2.0$ for both samples.

The top panel of Figure 11 compares these data to the prediction of the passive evolution model (Fry 1996), which significantly underpredicts the evolution of bias with redshift. Guo et al. (2013) compare the passive evolution model with the clustering of CMASS galaxies and find consistent result, but in a narrower redshift range of $0.47 < z < 0.62$. Using a much larger redshift range as Figure 11a, it highlights the deficiency of the passive evolving model to describe the clustering of massive galaxies. We also show a model in which the best-fit HOD from eBOSS+BOSS is used to predict the bias at the median redshift of each survey. This ansatz — that halo occupation of massive galaxies does not evolve — predicts more evolution in $b(z)$ than the passive model, but is still not a good description of the data especially at low redshift. Therefore some evolution is required for the full description from $z = 0.7$ to $z = 0$. The amount of bias evolution in the data implies that the HOD is evolving with time; namely, the scatter parameter $\sigma_{\log M}$ must increase with cosmic time to lower the bias at lower z . The dotted curve in top panel of Figure 11 shows a model in which the scatter in halo mass at fixed luminosity varies with redshift as

$$\sigma_{\log M}(z) = \sigma_{\log M}(z = 0.7) \left(\frac{1+z}{1+0.7} \right)^\beta \quad (12)$$

with $\beta \sim -0.3$, which yields a nearly linear fit to the $b(z)$ measurements.

Just because the scatter in halo mass at fixed luminosity varies with redshift does not necessarily imply that the scatter in luminosity at fixed halo mass ($\sigma_{\log L}$, here-

after) is also changing. To convert from one scatter to another requires the logarithmic slope of the halo mass function, which is also evolving with time. For galaxy formation theory, $\sigma_{\log L}$ is the more fundamental parameter, as it indicates how formation efficiency can vary at fixed gravitational potential. The lower panel in Figure 11 compares our $b(z)$ data to predictions from the abundance-matching model (see, e.g. Behroozi et al. 2013b and references therein). Here, we adopt the r -band luminosity function measured from the AGES survey Cool et al. (2012) to match galaxy luminosity onto halo mass. We use the high-resolution MultiDark N-body simulation presented in Riebe et al. (2011); Behroozi et al. (2013a,b), as well as the method presented in Wetzel & White (2010) to incorporate scatter at fixed halo mass. The data are consistent with a redshift-independent scatter of $\sigma_{\log L} = 0.19$, thus the change in $\sigma_{\log M}$ is entirely due to the evolution in the halo mass function and not due a change in the growth of stellar mass in massive objects over time. Moreover, Figure 11b highlights just how sensitive these data are to $\sigma_{\log L}$; the other curves show models in which $b(0.1) = 2.0$ — i.e., scatter is shrinking — and $b(0.1) = 1.5$, in which scatter increases with time. Our measurements imply $\sigma_{\log L} = 0.19 \pm 0.02$ with no redshift evolution.

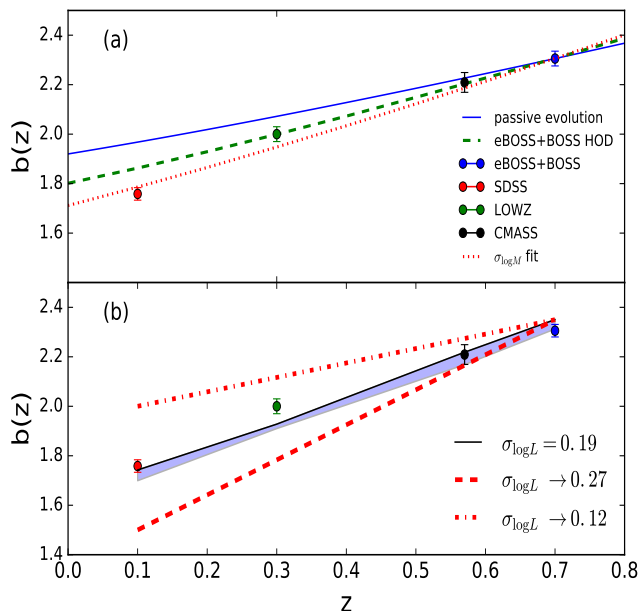


FIG. 11.— Measurements of bias based on the clustering studies. *Top panel* : Dynamical passive evolution model from eBOSS+BOSS LRGs (blue solid line). The green dashed line is the bias produced by placing the eBOSS+BOSS HOD at various redshifts. The red dotted line is obtained from the fit of the parameter $\sigma_{\log M}$ as explained in the context. *Bottom panel* : The interpretation of a constant scatter $\sigma_{\log L} = 0.19$ of these bias measurements (Solid). The blue shaded region corresponds to $\sigma_{\log L}$ between 0.19 and 0.20. Dashed and dot-dashed lines correspond to a linear evolution of $\sigma_{\log L}$ as a function of redshift z from $\sigma_{\log L} = 0.19$ at $z = 0.7$ to $\sigma_{\log L} = 0.27$ and $\sigma_{\log L} = 0.12$ at $z = 0.1$, respectively.

5. DISCUSSION AND CONCLUSION

This paper marks the first scientific results from the eBOSS LRG program. Although the observing strategy for eBOSS LRGs differs substantially from its predecessors in BOSS and SDSS, we have demonstrated that the combination of the bright-end of the BOSS CMASS sample with the eBOSS LRGs over the redshift range $0.6 < z < 0.9$ provides a robust clustering sample at small and intermediate scales. Our halo occupation analysis of this sample indicates that these galaxies have properties that are well-placed within our understanding of the relationship between massive galaxies and dark matter halos, with a bias factor of $b = 2.30$, a satellite fraction of $\sim 13\%$, and halo mass scale in agreement with the scaling relations calibrated on other surveys. The addition of the eBOSS galaxy sample to previous spectroscopic samples yields a set of massive galaxies that span that last ~ 7 Gyr of the history of the universe.

Our measurement of scatter in galaxy luminosity at fixed halo mass, $\sigma_{\log L} = 0.19 \pm 0.02$, is in good agreement with other studies that have focused on $z = 0$ samples. Lehmann et al. (2015), using galaxy clustering alone, reported a value of $0.17^{+0.03}_{-0.05}$; Reddick et al. (2013), using a combination of galaxy groups and clustering, find $0.21^{+0.01}_{-0.02}$; and More et al. (2009), using satellite kinematics, find 0.16 ± 0.04 . Assuming these measurements are all independent (which is not strictly true), the weighted combination of all four results indicate $\sigma_{\log L} = 0.19 \pm 0.01$, a value that is somewhat larger than recent measurements of the scatter in stellar mass at fixed halo mass, $\sigma_{\log M_*} \approx 0.16$ (Li et al. 2012; Kravtsov et al. 2014; Tinker et al. 2016; Zu & Mandelbaum 2016), which itself appears to be independent of redshift. The larger scatter in luminosity, for galaxies that are nearly all on the red sequence, is indicative of different formation histories at fixed stellar mass that yield different stellar- M/L ratios and mean stellar ages.

At first glance, the lack of evolution of either scatter value is notable but not surprising given that the massive end of the red sequence is constructed prior to $z \sim 1$ and that massive galaxies evolve in a manner close to passive stellar evolution over that timespan (Wake et al. 2008; Cool et al. 2008). However, true passive evolution of massive galaxies would result in a reduction in $\sigma_{\log L}$ as galaxies evolve, due to the fact that M/L ratios for passive stellar populations evolve to the same asymptotic value. To match dynamically passive evolution, $\sigma_{\log L}$ would have to decrease from 0.19 at $z = 0.7$ to 0.12 at $z = 0.1$, which is clearly ruled out by our measurements. Gu et al. (2016) find that the scatter (in stellar mass) induced by hierarchical merging is constant with redshift, but merging is not the dominant source of scatter at the halo masses probed by eBOSS galaxies. For galaxies in $10^{13} h^{-1} M_{\odot}$ halos, in-situ star formation is still predicted to be the dominant source of scatter. Abundance-matching studies by Behroozi et al. (2013a) and Moster et al. (2013) demonstrate that stellar mass growth from merging accounts for $\sim 10\%$ of the $z = 0$ galaxy mass. This result is in agreement with earlier clustering studies of massive galaxies that found LRG merger rates of $\sim 1\%$ per Gyr (Wake et al. 2008 and references therein). How does a population without merging or star formation have a constant luminosity scatter for over half the lifetime of the universe?

SDSS, CMASS, LOWZ, and eBOSS represent a heterogeneous set of galaxy samples. Our SDSS sample is volume-limited, and at $M_r < -21.7$ the fraction of star-forming objects is negligible. The BOSS samples, as a whole, suffer from high significant incompleteness due to their color-based selections (Leauthaud et al. 2016; Tinker et al. 2016), but by using only the brightest third of each sample in relatively narrow redshift ranges, CMASS and LOWZ are roughly complete as well. eBOSS, however, cannot be considered a complete sample. It is not trivial to estimate what the bias of a complete eBOSS sample would be at the number density used to create our subsamples, $1.4 \times 10^{-4} (h^{-1} \text{Mpc})^{-3}$. The color selection excludes some brighter galaxies and includes some fainter objects, but the fainter objects will be redder and thus possibly more clustered than the brighter, but bluer, excluded objects. This is true of the overall CMASS sample (c.f. Figure 7 of Tinker et al. 2016). If this is true of eBOSS, then the overall trend of $b(z)$ in Figure 11 would be consistent with some small reduction in $\sigma_{\log L}$ with time. Alternatively, the scatter in stellar M/L -ratio on the red sequence may not change enough between $z = 0.7$ and $z = 0.1$ to be detectable within our precision of 0.02 dex in scatter, since this scatter would add in quadrature with the scatter in stellar mass at fixed halo mass. Stellar population synthesis models would be required to address this question within the precision of our measurements, and will be included in a future work.

The primary science driver of the eBOSS LRG sample is to probe the growth and expansion history of the universe at $z = 0.7$. As a part of the SDSS-IV project, the eBOSS survey takes over the mission from its precursor BOSS and will map the universe in a higher redshift range and larger volume. After roughly one year observation, we reach a LRG sample with more than 34000 massive galaxies at an effective redshift $z \sim 0.7$. The result here shows that eBOSS is working well and the designed expectation is being reached. The clustering measurements that will be achieved with this sample through the completion of this survey will an important extension

toward a complete map of the observable universe.

We thank Peter Behroozi for having his Rockstar DM halo catalogs publicly available, as well as Pierre Laurent for his kind help. H.-J. Seo is supported by the U.S. Department of Energy, Office of Science, Office of High Energy Physics under Award Number DE-SC0014329.

Funding for the Sloan Digital Sky Survey IV has been provided by the Alfred P. Sloan Foundation, the U.S. Department of Energy Office of Science, and the Participating Institutions. SDSS-IV acknowledges support and resources from the Center for High-Performance Computing at the University of Utah. The SDSS web site is www.sdss.org.

SDSS-IV is managed by the Astrophysical Research Consortium for the Participating Institutions of the SDSS Collaboration including the Brazilian Participation Group, the Carnegie Institution for Science, Carnegie Mellon University, the Chilean Participation Group, the French Participation Group, Harvard-Smithsonian Center for Astrophysics, Instituto de Astrofísica de Canarias, The Johns Hopkins University, Kavli Institute for the Physics and Mathematics of the Universe (IPMU) / University of Tokyo, Lawrence Berkeley National Laboratory, Leibniz Institut für Astrophysik Potsdam (AIP), Max-Planck-Institut für Astronomie (MPIA Heidelberg), Max-Planck-Institut für Astrophysik (MPA Garching), Max-Planck-Institut für Extraterrestrische Physik (MPE), National Astronomical Observatory of China, New Mexico State University, New York University, University of Notre Dame, Observatório Nacional / MCTI, The Ohio State University, Pennsylvania State University, Shanghai Astronomical Observatory, United Kingdom Participation Group, Universidad Nacional Autónoma de México, University of Arizona, University of Colorado Boulder, University of Oxford, University of Portsmouth, University of Utah, University of Virginia, University of Washington, University of Wisconsin, Vanderbilt University, and Yale University.

APPENDIX

BRIGHT STAR MASK

To investigate the effect of the bright stars on the LRG clustering, we apply the latest bright star mask which is designed for eBOSS tiling process to our clustering measurements. The bright source catalog used for the analysis is based on the WISE Allsky catalog¹⁹. All the sources with at least one saturated pixel are selected.

In order to present the influence of the bright star mask, we calculate the following quantity

$$f(r_p) = \frac{w_{p2}(r_p) - w_{p1}(r_p)}{w_{p1}(r_p)}, \quad (\text{A1})$$

where w_{p2} and w_{p1} are the projected correlation functions for LRG with and without applying the bright star mask respectively. We assess the value of this fractional difference f through tens of random catalogs which have different sizes and seeds. Figure 12 presents the average and 1σ error of f from ten different realizations of random catalogs. This result shows that the effect of bright star mask is no more than 5% at all scales. This deviation is therefore believed to be noise dominated and not significant. The HOD interpretation of the clustering measurement due to the bright star mask is still valid since the HOD parameters have no essential change.

TILED MOCK TEST

The effect of the fiber allocation on our clustering measurement is tested with a mock catalog. This mock is put into the same tiling process as the eBOSS survey. The resulting catalog has the same survey geometry, redshift distribution

¹⁹ <http://wise2.ipac.caltech.edu/docs/release/allsky/>

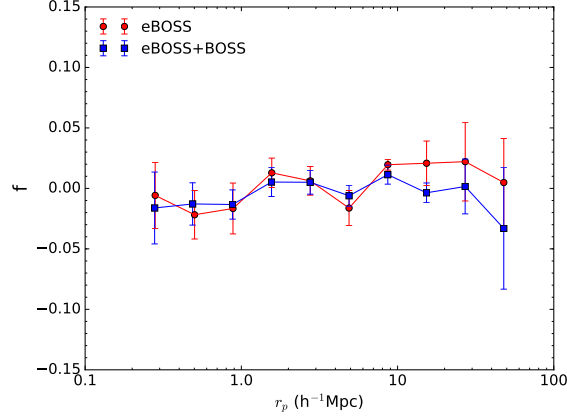


FIG. 12.— The effect of the bright star mask on the clustering measurements. It is represented by the fractional difference of the projected correlation w_p with and without applying the bright star mask. Both the eBOSS and eBOSS+BOSS LRG samples are shown, and the effect is found to be smaller than 5% at all scales.

and target density as the LRG sample. Therefore we apply the same angular correction method to this sample; the result is shown in the left panel of Figure 13. The consistency between the intrinsic clustering and the recovered clustering is clear, thus validating our measurement method. For comparison, we also test this correction method for the BOSS CMASS mock (right panel) which reveals the same robustness.

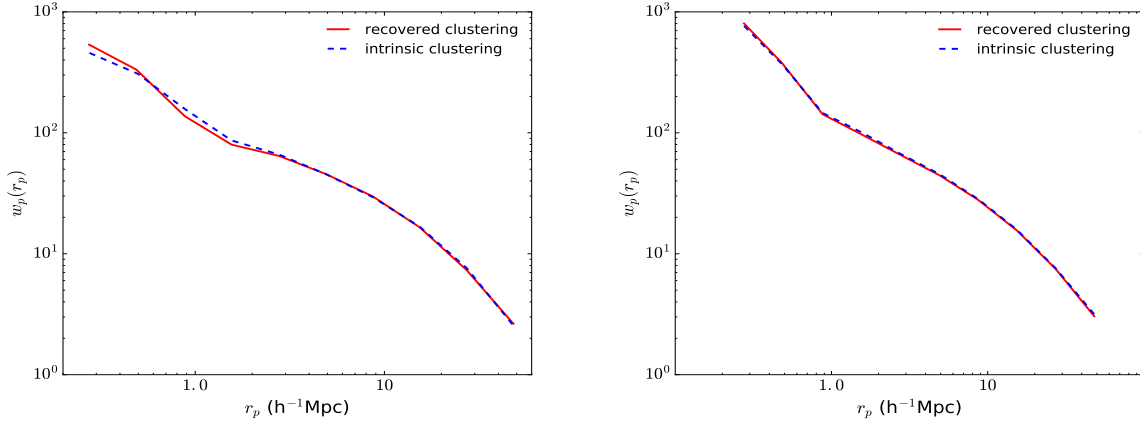


FIG. 13.— The clustering measurement from the tiled mock. The intrinsic clustering is also shown for comparison. The recovered clustering is measured by the correction method as described in Section 3. The consistency between these results especially in small scales approves our method to measure the correlation function. *Leftpanel* : eBOSS; *Rightpanel* : BOSS

REFERENCES

- Abazajian, K., Adelman-McCarthy, J. K., Agüeros, M. A., et al. 2004, *AJ*, 128, 502
- Anderson, L., Aubourg, E., Bailey, S., et al. 2012, *MNRAS*, 427, 3435
- Behroozi, P. S., Wechsler, R. H., & Wu, H.-Y. 2013a, *ApJ*, 762, 109
- Behroozi, P. S., Wechsler, R. H., Wu, H.-Y., et al. 2013b, *ApJ*, 763, 18
- Benson, A. J., Cole, S., Frenk, C. S., Baugh, C. M., & Lacey, C. G. 2000, *Monthly Notices of the Royal Astronomical Society*, 311, 793
- Berlind, A. A., & Weinberg, D. H. 2002, *The Astrophysical Journal*, 575, 587
- Bolton, A. S., Schlegel, D. J., Aubourg, É., et al. 2012, *AJ*, 144, 144
- Cole, S., Percival, W. J., Peacock, J. A., et al. 2005, *Monthly Notices of the Royal Astronomical Society*, 362, 505
- Cool, R. J., Eisenstein, D. J., Fan, X., et al. 2008, *ApJ*, 682, 919
- Cool, R. J., Eisenstein, D. J., Kochanek, C. S., et al. 2012, *ApJ*, 748, 10
- Cooray, A., & Sheth, R. 2002, *Physics Reports*, 372, 1
- Davis, M., & Peebles, P. J. E. 1983, *ApJ*, 267, 465
- Dawson, K. S., Schlegel, D. J., Ahn, C. P., et al. 2013, *The Astronomical Journal*, 145, 10
- Dawson, K. S., Kneib, J.-P., Percival, W. J., et al. 2016, *AJ*, 151, 44
- Eisenstein, D. J., Zehavi, I., Hogg, D. W., et al. 2005, *The Astrophysical Journal*, 633, 560
- Eisenstein, D. J., Weinberg, D. H., Agol, E., et al. 2011, *AJ*, 142, 72
- Fisher, K. B., Davis, M., Strauss, M. A., Yahil, A., & Huchra, J. 1994, *Monthly Notices of the Royal Astronomical Society*, 266, 50
- Fry, J. N. 1996, *The Astrophysical Journal Letters*, 461, L65
- Fukugita, M., Ichikawa, T., Gunn, J. E., et al. 1996, *AJ*, 111, 1748

- Gu, M., Conroy, C., & Behroozi, P. 2016, ArXiv e-prints, arXiv:1602.01099
- Gunn, J. E., Siegmund, W. A., Mannery, E. J., et al. 2006, *AJ*, 131, 2332
- Guo, H., Zehavi, I., Zheng, Z., et al. 2013, *ApJ*, 767, 122
- Guo, H., Zheng, Z., Zehavi, I., et al. 2014, *MNRAS*, 441, 2398
- Hawkins, E., Maddox, S., Cole, S., et al. 2003, *Monthly Notices of the Royal Astronomical Society*, 346, 78
- Hutchinson, T., et al. 2016, in preparation
- Kravtsov, A., Vikhlinin, A., & Meshcheryakov, A. 2014, *ApJ*, submitted, arXiv:1401.7329, arXiv:1401.7329
- Landy, S. D., & Szalay, A. S. 1993, *ApJ*, 412, 64
- Leauthaud, A., Bundy, K., Saito, S., et al. 2016, *MNRAS*, 457, 4021
- Lehmann, B. V., Mao, Y.-Y., Becker, M. R., Skillman, S. W., & Wechsler, R. H. 2015, ArXiv e-prints, arXiv:1510.05651
- Li, C., Jing, Y. P., Mao, S., et al. 2012, *ApJ*, 758, 50
- Macciò, A. V., Dutton, A. A., & van den Bosch, F. C. 2008, *MNRAS*, 391, 1940
- More, S., van den Bosch, F. C., Cacciato, M., et al. 2009, *MNRAS*, 392, 801
- Moster, B. P., Naab, T., & White, S. D. M. 2013, *MNRAS*, 428, 3121
- Navarro, J. F., Frenk, C. S., & White, S. D. M. 1996, *ApJ*, 462, 563
- Norberg, P., Baugh, C. M., Gaztaaga, E., & Croton, D. J. 2009, *Monthly Notices of the Royal Astronomical Society*, 396, 19
- Parejko, J. K., Sunayama, T., Padmanabhan, N., et al. 2013, *Monthly Notices of the Royal Astronomical Society*, 429, 98
- Peacock, J. A., & Smith, R. E. 2000, *Monthly Notices of the Royal Astronomical Society*, 318, 1144
- Peebles, P. J. E. 1980, *The large-scale structure of the universe* (Princeton university press)
- Prakash, A., Licquia, T. C., Newman, J. A., et al. 2016, *ApJS*, 224, 34
- Reddick, R. M., Wechsler, R. H., Tinker, J. L., & Behroozi, P. S. 2013, *ApJ*, 771, 30
- Riebe, K., Partl, A. M., Enke, H., et al. 2011, ArXiv e-prints, arXiv:1109.0003
- Seljak, U. 2000, *Monthly Notices of the Royal Astronomical Society*, 318, 203
- Smee, S. A., Gunn, J. E., Uomoto, A., et al. 2013, *AJ*, 146, 32
- Stoughton, C., Lupton, R. H., Bernardi, M., et al. 2002, *AJ*, 123, 485
- Swanson, M. E. C., Tegmark, M., Hamilton, A. J. S., & Hill, J. C. 2008, *Monthly Notices of the Royal Astronomical Society*, 387, 1391
- Tinker, J., Kravtsov, A. V., Klypin, A., et al. 2008, *ApJ*, 688, 709
- Tinker, J., et al. 2016, ArXiv e-prints, arXiv:1607.04678
- Tinker, J. L., Robertson, B. E., Kravtsov, A. V., et al. 2010, *ApJ*, 724, 878
- Tinker, J. L., Weinberg, D. H., Zheng, Z., & Zehavi, I. 2005, *The Astrophysical Journal*, 631, 41
- Tinker, J. L., Sheldon, E. S., Wechsler, R. H., et al. 2012, *ApJ*, 745, 16
- Wake, D. A., Sheth, R. K., Nichol, R. C., et al. 2008, *MNRAS*, 387, 1045
- Wetzel, A. R., & White, M. 2010, *MNRAS*, 403, 1072
- White, M., Hernquist, L., & Springel, V. 2001, *The Astrophysical Journal Letters*, 550, L129
- White, M., Tinker, J. L., & McBride, C. K. 2014, *Monthly Notices of the Royal Astronomical Society*, 437, 2594
- White, M., Blanton, M., Bolton, A., et al. 2011, *The Astrophysical Journal*, 728, 126
- Wright, E. L., Eisenhardt, P. R. M., Mainzer, A. K., et al. 2010, *AJ*, 140, 1868
- Zehavi, I., Blanton, M. R., Frieman, J. A., et al. 2002, *The Astrophysical Journal*, 571, 172
- Zehavi, I., Zheng, Z., Weinberg, D. H., et al. 2005, *The Astrophysical Journal*, 630, 1
- Zehavi, I., Zheng, Z., Weinberg, D. H., et al. 2011, *ApJ*, 736, 59
- Zhao, G.-B., Wang, Y., Ross, A. J., et al. 2016, *MNRAS*, 457, 2377
- Zheng, Z., Coil, A. L., & Zehavi, I. 2007, *The Astrophysical Journal*, 667, 760
- Zheng, Z., Zehavi, I., Eisenstein, D. J., Weinberg, D. H., & Jing, Y. P. 2009, *ApJ*, 707, 554
- Zu, Y., & Mandelbaum, R. 2016, *MNRAS*, 457, 4360